Shape coexistence in Sr isotopes

E. Maya-Barbecho [1] and J. E. García-Ramos [1,2]
[1]*Departamento de Ciencias Integradas y Centro de Estudios Avanzados en Física, Matemática y Computación, Universidad de Huelva, 21071 Huelva, Spain*
[2]*Instituto Carlos I de Física Teórica y Computacional, Universidad de Granada, Fuentenueva s/n, 18071 Granada, Spain*

(Received 17 December 2021; accepted 8 March 2022; published 29 March 2022)

Background: Sr isotopes are located in the mass region $A \approx 100$, where a very quick onset of nuclear deformation exists; other notable examples of this area are Yb, Zr, and Nb nuclei. The presence of the proton subshell closure $Z = 40$ allows the existence of particle-hole excitations that produce low-lying intruder bands.
Purpose: The goal of this work is the study of the nuclear structure of the even-even $^{92-102}$Sr isotopes through the accurate description of excitation energies, $B(E2)$ transition rates, nuclear radii, and two-neutron separation energies.
Method: The interacting boson model with configuration mixing will be the framework to calculate all the observables of the Sr isotopes. Only two types of configurations will be considered, namely, 0-particle–0-hole and 2-particle–2-hole excitations. The parameters of the model are determined using a least-squares procedure for the excitation energies and the $B(E2)$ transition rates.
Results: For the whole chain of isotopes, the value of excitation energies, $B(E2)$'s, two-neutron separation energies, nuclear radii, and isotope shifts have been obtained, with a good agreement between theory and experiment. Also, a detailed analysis of the wave functions have been performed and, finally, the mean-field energy surfaces and the value of the nuclear deformation, β, have been obtained.
Conclusions: The presence of low-lying intruder states in even-even Sr isotopes has been confirmed and its connection with the onset of deformation has been clarified. The lightest Sr isotopes present a spherical structure while the heaviest ones are clearly deformed. The rapid onset of deformation at neutron number 60 is due to the crossing of the regular and intruder configurations and, moreover, both families of states present an increase of deformation with the neutron number.

DOI: 10.1103/PhysRevC.105.034341

I. INTRODUCTION

Nuclear deformation plays a major role in the understanding of the evolution of nuclear structure along the mass table. The shape of the nucleus is determined by a fine balance between, on one hand, the stabilizing effect of closed shells that tends to make the nucleus exhibit properties of spherical shape, and, on the other, the pairing and the quadrupole force that tend to make the nucleus quadrupole deformed [1]. This balance generates regions near closed shells with spherical shapes, while those around mid-shell are well deformed. In particular, the evolution of the single-particle levels (monopole term) and the strength of the rest of the low multipolar terms of the nuclear interaction are key elements for a correct understanding of the nuclear shape. The correct description of the transition from one limit to the other remains at present a major issue in theoretical nuclear physics.

The situation is even more appealing when in the nuclear spectrum states coexist with different shapes in a narrow energy range. This phenomenon is named shape coexistence and in nuclear physics it was first proposed by Morinaga [2] to explain the nature of the first excited state in ^{16}O, a 0^+ state which was assumed to be deformed, although the ground state is obviously spherical because the nucleus is doubly magic. This state corresponds to a proton 2p-2h excitation across the $Z = 8$ shell closure and, therefore, it is a intruder state with a deformed structure. This idea was also supported by the early works [3–5] for oxygen isotopes. In closed nuclei, such as ^{16}O, both proton and neutron excitations across magic number 8 appear as the major component of the structure of the first 0^+ state and lead naturally, through the effect of the quadrupole part of the nucleon-nucleon interactions, to the existence of a deformed band built on top of this 0^+ (called an intruder). This becomes a major indication for the appearance of shapes with an unexpected feature in nuclei that contain doubly magic proton and neutron configurations. One of the most explicit examples of such shape coexistence is observed experimentally in ^{40}Ca and is very well described through shell model calculations involving mp-nh excitations [6–8].

Experimentally, the most dramatic example of shape coexistence is provided by the systematics of nuclear radii and the isotope shifts observed in certain mass regions. The existence of sudden changes in those observables hint to the presence of intruder states that affect the deformation of the ground state. In particular, that was first observed in the case of Hg where the odd-even staggering in the radius systematics

clearly points to the presence of states with rather different degrees of deformation. Since then, shape coexistence has been found to play a major role to explain the nuclear structure in many mass regions, especially in those close to a shell or subshell closure in protons (neutrons) and around the mid-shell in neutrons (protons), being present in light, medium, and heavy nuclei [9–11].

The theoretical description of shape coexistence can be done with two complementary approaches, namely, the nuclear shell model and the self-consistent way, based on Hartree-Fock (HF) or Hartree-Fock-Bogoliubov (HFB) theories. The residual interaction used in the shell-model Hamiltonian has been refined in recent decades, as shown in [12] where a new universal interaction for the *sd* shell was designed or in [13] where the interaction was obtained for the *sd*-*pf* shell. The description of the region around $Z = 40$ is driven by the simultaneous occupation of neutrons and protons in spin-orbit partners. Hence, once the neutron $1g_{7/2}$ orbit starts to be filled, the interaction with the proton $1g_{9/2}$ orbit favors the existence of a zone of deformation in Zr and Sr nuclei with neutron number larger than 58. This idea was proposed in the seminal works of Federman and Pittel [14–16], entitled "A unified shell-model description of nuclear deformation," where the key importance of the simultaneous occupation of the neutron-proton spin-orbit partners is emphasized. Federman and coworkers explored in depth this mass area using a reduced model space consisting of the $3s_{1/2}$, $2d_{3/2}$, and $1g_{7/2}$ neutron orbits and, in the case of protons, the $2p_{1/2}$, $1g_{9/2}$, and $2d_{5/2}$ orbits [17–20]. More recently, large scale shell-model calculations have been performed for the same mass region using more realistic valence spaces, as in the case of [21] or [22]. However, in order to correctly treat the possible existence of *n*p-*n*h excitations across the $Z = 40$ shell gap, one needs to include other shells, thereby rapidly increasing the size of the model space, exceeding present computational capabilities. To overcome this limitation, the Monte Carlo shell model was introduced by Otsuka *et al.* [23] and Shimizu *et al.* [24,25] and it has been successfully applied to the Zr region [26]. In this work, the filling of the proton $1g_{9/2}$ shell was observed either for the ground state or for low-lying excited states.

The other mainstream approach to deal with shape coexistence and configuration mixing is the mean-field approach. In [27], the authors studied the rapid change in the structure of Sr an Zr isotopes, solving a five-dimensional collective Hamiltonian with parameters coming from a nonrelativistic Skyrme interaction and the PC-PK1 and SLy4 relativistic forces. A spherical-oblate-prolate shape transition in neutron-rich Sr and Zr isotopes is observed. In [28], the authors studied Kr, Sr, Zr, and Mo isotopes around neutron number 60 with the relativistic interaction PC-PK1. A rapid evolution in Sr and Zr, while moderated in Mo and Kr, is observed, in addition to a prolate-oblate shape coexistence in ^{98}Sr and ^{100}Zr. In [29], the even-even Ru, Mo, Zr, and Sr are studied within the HFB approach using a Gogny-D1M interaction. The different spectroscopic properties are obtained thanks to the mapping of the energy density functional into an interacting boson model with configuration mixing (IBM-CM) energy surface. In the case of Sr as in the case of Zr, there is a rapid change in the structure of the 0_1^+ and 0_2^+ states when approaching neutron number 60. The spectroscopic properties of Zr and Sr isotopes, among many others, were obtained in [30] using a generalized Bohr Hamiltonian in which parameters are fixed through a reduction of the Hill-Wheeler generator coordinate method equation using a Gaussian overlap approximation (GOA). In [31], the experimental information for Zr isotopes is compared with the theoretical results obtained with three different approaches, namely, the GOA reduction to the five-dimensional Bohr Hamiltonian, the solutions of the Hill-Weeler equations using the SLyMR00 version of the Skyrme force, or using a Gogny D1S interaction. All the approaches provide a good description of the energy systematics of the 2_1^+ state, but differences are shown up for the energy ratio $E(4_1^+)/E(2_1^+)$. Calculations that represent the state of the art of the field were carried out by Rodríguez-Guzmán *et al.* [32] within the HFB framework, allowing them to handle both the axial and triaxial degrees of freedom on equal footing, with full symmetry conserving configuration mixing calculations and with application to Sr, Zr, and Mo.

The present work extends our previous analysis of the $Z \approx 40$ and $A \approx 100$ region [33,34], in particular the even-even Zr isotopes, to the case of Sr. Sr is also an excellent candidate to study the influence of the intruder states on the onset of deformation for $N \approx 60$ because it presents a rapid lowering of the energy of the 2_1^+ state, a rapid growing of the ratio $E(4_1^+)/E(2_1^+)$, a sudden increase in the radius, or a flatness of the two-neutron separation energy.

The paper is organized as follows. In Sec. II, the present experimental knowledge on Sr is reviewed; in Sec. III, we present the theoretical framework of this work, i.e., the IBM-CM, including the procedure used to get the fitting parameters of the model; in Sec. IV, the study of the correlation energy gain is presented; in Sec. V, a detailed comparison of theory and experiment is presented; in Sec. VI, the analysis of the wave functions is given; in Sec. VII, we study the radii, the isotopic shifts, and the two-neutron separation energies; in Sec. VIII, we calculate the mean-field energy surfaces and deformations; and, finally, in Sec. IX the summary and the conclusions are presented.

II. EXPERIMENTAL DATA IN THE EVEN-EVEN Sr NUCLEI

The experimental knowledge of even-even Sr isotopes in the neutron 50–82 shell spans from the closed-shell nucleus ^{88}Sr to the deformed one ^{102}Sr, as depicted in Fig. 1, where the energy systematics of positive-parity states up to an excitation energy $E \approx 3$ MeV is presented. For these isotopes there is a clear need for more experimental data and, in particular, for the use of complementary techniques to extract information on quadrupole moments using Coulomb excitation methods and lifetime measurements. The experimental data on $\rho^2(E0)$ will lead to direct information concerning shape mixing, as has been shown in the nearby Zr isotopes and many other regions. In Fig. 1 we used blue and red colors for the states whose structure as been established firmly in the recent literature as being regular (vibrational-like) or intruder (rotational-like), respectively, as discussed in detail below.

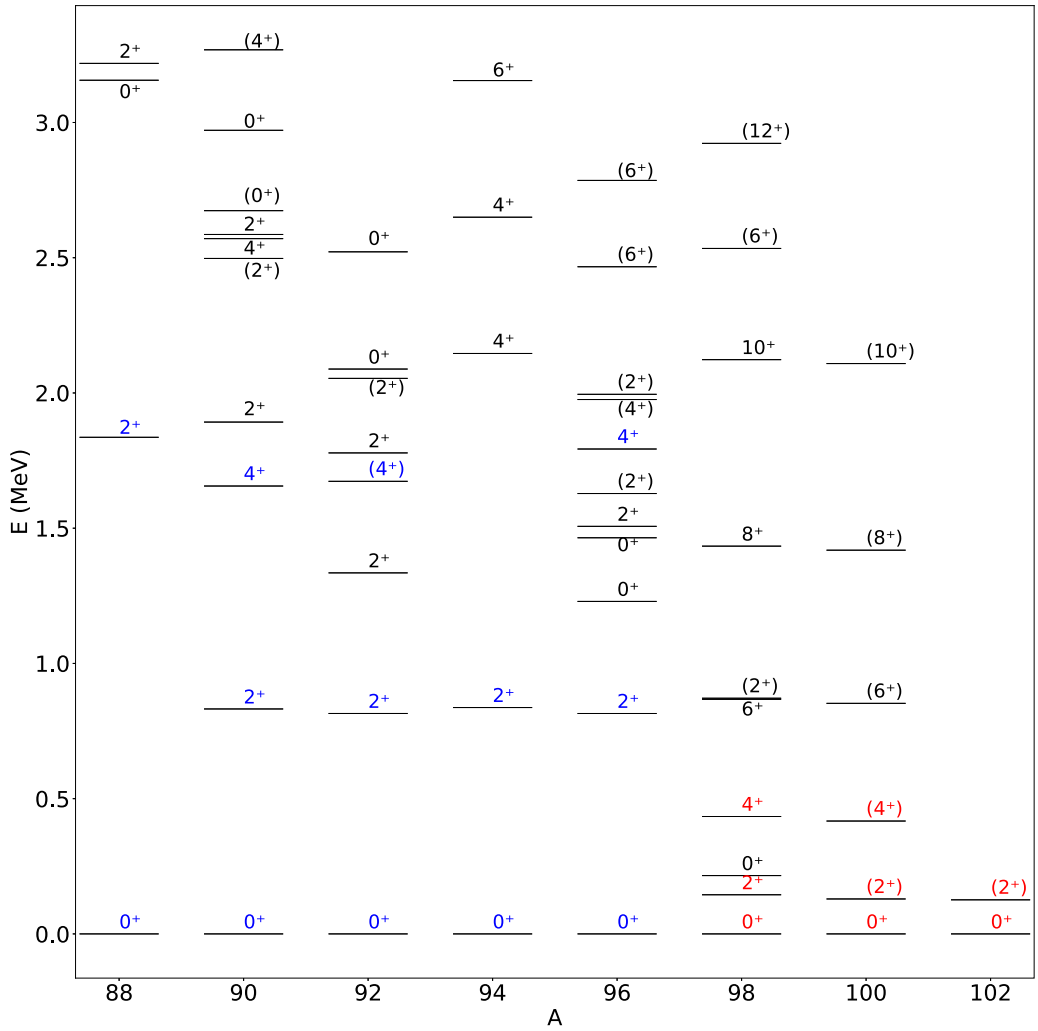

FIG. 1. Experimental energy level systematics of positive parity states for the Sr isotopes. Only levels up to $E_x \approx 3$ MeV are shown. Levels labeled in blue correspond to spherical shapes, those labeled in red to deformed ones (see information in Sec. II).

The nucleus ^{88}Sr is characterized by a large energy gap between the ground state and the first excited one, a 2^+ state, as it corresponds to the shell closure; in $^{90-92}$Sr an underlying vibrational spectrum is seen although it becomes much more complex as the energy increases; in ^{94}Sr the energy of the 2_1^+ state remains constant but a large energy gap appears with the 4_1^+ state; when passing from ^{96}Sr to ^{98}Sr the spectrum is suddenly compressed with a much smaller $E(2_1^+)$; and for $^{100-102}$Sr only the yrast band is observed with a clear rotational structure.

For comparison with theoretical calculations, we have considered, when available, the evaluated experimental data appearing in Nuclear Data Sheets publications for $A = 92$ [35], $A = 94$ [36,37], $A = 96$ [38], $A = 98$ [39,40], $A = 100$ [41], and $A = 102$ [42], complemented with the most up to date references for certain isotopes. Note that we do not consider in our analysis the nuclei $^{88-90}$Sr because they are at or too close to the shell closure, where our theoretical approach is not reliable enough.

In [43] the isotopes ^{92,94,96}Sr were studied through the spontaneous fission of ^{248}Cm, and new spin and parity were assigned to several energy levels, which differ from previous works. Park *et al.* [44] conducted a γ-ray and internal conversion electron spectroscopy experiment for ^{98}Sr at the TRIUMF-ISAC facility. In this work, the $\rho^2(E0)$ value for the transition $0_2^+ \rightarrow 0_1^+$ and the $B(E2)$ values for $2_1^+ \rightarrow 0_1^+$, $0_2^+ \rightarrow 2_1^+$, and $4_1^+ \rightarrow 2_1^+$ transitions were obtained and, except for the case of the $B(E2; 0_2^+ \rightarrow 2_1^+)$ transition, the obtained values were compatible with the evaluated ones. The obtained mixing for the first two 0^+ states was 9% while for the two 2^+ states it was 1.3%. In [45], the authors have investigated the neutron-rich ^{96,98}Sr isotopes using Coulomb excitation at the REX-ISOLDE facility (CERN). $B(E2)$'s and spectroscopic quadrupole moments were extracted from the cross sections. A small mixing is obtained between a spherical and a prolate configuration in ^{98}Sr. In [46], the authors conducted an experiment for neutron-rich Sr isotopes using Coulomb excitation with radioactive beams at the REX-ISOLDE facility (CERN)

using the MINIBALL spectrometer. They concluded that there is a sudden increase in the value of β for ^{98}Sr with a mixing between regular and intruder states of only a 12%. In [47], the authors measured the lifetime of the isotopes ^{94,96,98}Sr using LaBr3(Ce) detectors combined with Ge ones in the EXILL-FATIMA spectrometer at the Institut Laue-Langevin in Grenoble. They obtained values for transition rates in the yrast band up to $J = 6^+$, observing the rapid onset of deformation in ^{98}Sr. In [48], the spectroscopic factors of $0^+_{2,3}$ states were determined for ^{96}Sr and the results are consistent with a 40% mixing and a difference in β between both 0^+ states of 0.31. In [49], delayed γ rays in $A = 97$ fission fragments were analyzed too at the high flux nuclear reactor of the Institute Laue-Langevin in Grenoble. Several lifetimes for ^{97}Sr were measured using a fast-timing setup. This nucleus is at the spherical-deformed border, i.e., between neutron numbers 58 and 60, the place where Sr isotopes pass from being spherical to deformed. Urban *et al.* [50] studied the 0^+_2 states of ^{98}Sr and ^{100}Zr by analyzing the spontaneous fission of ^{248}Cm and ^{252}Cf in the Eurogam2 and the Gammasphere arrays; moreover, in this work they classified phenomenologically the 0^+ states into four categories, concluding that the first two 0^+ states are highly deformed and correspond to 2p-2h excitations of two neutrons from the $9/2^+[404]$ extruder level to the low-Ω prolate and the $11/2^-[505]$ oblate orbitals originating from the $h_{11/2}$ shell. More recently, the same group [51] reinvestigated the excited states of ^{90,92,94,96,98}Sr using the Exogam and Gammasphere arrays. Twenty-three new levels with 30 new decays were obtained in four nuclei. Finally, in [52], the authors studied the level structure of ^{93,94,95}Sr via one-neutron stripping reactions at TRIUMF. The results suggest a strong mixing in ^{94}Sr and in ^{96}Sr, showing indications of shape transition before $N = 60$. Of relevance are the observations in ^{94}Sr of two 0^+ states at 1880 and 2293 keV (not considered in this work)

III. THE INTERACTING BOSON MODEL WITH CONFIGURATION MIXING FORMALISM

A. The formalism

The IBM-CM supposes an extension of the original formulation of the IBM [53] and it allows the simultaneous treatment of several boson configurations corresponding to particle-hole excitations across a shell or subshell closure [54,55]. In this version of the model no distinction is made between proton and neutron bosons. In the case of Sr, this shell closure is assumed to exist for $Z = 40$, associating the regular states to a 2h proton configuration and the intruder ones to a 4h-2p proton configuration, and the number of valence neutrons is determined considering 50 as the neutron closed shell. Therefore, the number of valence bosons, N, will be half of the sum of the valence protons, which is 2, plus half the number of valence neutrons. The intruder configuration will own, in addition, two extra bosons. Hence, the regular plus the intruder space will correspond to an $[N] \oplus [N+2]$ Hilbert space. The Hamiltonian will be made of two sectors—one corresponding to the regular part, $[N]$, another to the intruder one, $[N+2]$—and an interaction term, with the total Hamiltonian being written as

$$\hat{H} = \hat{P}^\dagger_N \hat{H}^N_{\rm ecqf} \hat{P}_N + \hat{P}^\dagger_{N+2} \big(\hat{H}^{N+2}_{\rm ecqf} + \Delta^{N+2}\big) \hat{P}_{N+2} + \hat{V}^{N,N+2}_{\rm mix}, \tag{1}$$

where $\hat{P}_N$ and $\hat{P}_{N+2}$ are projection operators onto the $[N]$ and the $[N+2]$ boson spaces, respectively,

$$\hat{H}^i_{\rm ecqf} = \varepsilon_i \hat{n}_d + \kappa'_i \hat{L} \cdot \hat{L} + \kappa_i \hat{Q}(\chi_i) \cdot \hat{Q}(\chi_i) \tag{2}$$

is a simplified IBM Hamiltonian named the extended consistent-Q Hamiltonian (ECQF) [56,57] with $i = N, N+2$ and with $\hat{n}_d$ the d boson number, $\hat{L}$ the angular momentum, and $\hat{Q}(\chi)$ the quadrupole operator. The parameter Δ^{N+2} represents the energy needed to excite two proton particles across the $Z = 40$ shell gap, giving rise to 2p-2h excitations, corrected with the pairing interaction gain and including monopole effects [58,59]. The operator $\hat{V}^{N,N+2}_{\rm mix}$ describes the mixing between the N and the $N+2$ configurations and is defined as

$$\begin{aligned}\hat{V}^{N,N+2}_{\rm mix} = {} & \omega^{N,N+2}_0 (s^\dagger \times s^\dagger + s \times s) \\ & + \omega^{N,N+2}_2 (d^\dagger \times d^\dagger + \tilde{d} \times \tilde{d})^{(0)}.\end{aligned} \tag{3}$$

In this work, we assume $\omega^{N,N+2}_0 = \omega^{N,N+2}_2 = \omega$.

The $E2$ transition operator is built with the same quadrupole operator that appears in the Hamiltonian (2) and it is defined as the sum of two contributions that act separately in the regular and the intruder sectors without crossed contributions,

$$\hat{T}(E2)_\mu = \sum_{i=N,N+2} e_i \hat{P}^\dagger_i \hat{Q}_\mu(\chi_i) \hat{P}_i. \tag{4}$$

The e_i ($i = N, N+2$) are the effective boson charges and the parameters χ_i take the same values as in the Hamiltonian (2).

In the previously defined operators there is a set of free parameters that should be fixed to reproduce as well as possible a set of excitation energies and transition rates, as will be explained in detail in Sec. III B.

This approach has been successfully used in a set of recent works for Zr [33,34], Pt [60,61], Hg [62,63], and Po isotopes [64,65].

B. The fitting procedure: Energy spectra and absolute $B(E2)$ reduced transition probabilities

In this section, we present the way the parameters of the Hamiltonian (1), (2), and (3) as well as the effective charges of the $\hat{T}(E2)$ transition operator (4) have been fixed.

We study in this work the even-even isotopes $^{92-102}$Sr, thereby covering almost the whole first half of the neutron shell 50–82. Note that we do not consider the isotopes $^{88-90}$Sr because they are too close to the neutron shell closure, 50, and therefore the IBM calculations are not reliable enough.

In the fitting procedure carried out here, we try to obtain the best overall agreement with the experimental data including both the excitation energies and the $B(E2)$ reduced transition probabilities. A standard χ^2 is used to obtain the free parameters of the Hamiltonian and the $\hat{T}(E2)$ operator as described in [33,60,62,64]. Using the expression of the IBM-CM Hamiltonian, as given in Eq. (1), and of the $E2$ operator, as given in Eq. (4), in the most general case 13 parameters show up.

TABLE I. Hamiltonian and $\hat{T}(E2)$ parameters resulting from the present study. All quantities have the dimension of energy (given in keV), except χ_N and χ_{N+2} which are dimensionless and e_N and e_{N+2} which are given in units $\sqrt{\text{W.u.}}$.

Nucleus	N	ε_N	κ_N	χ_N	κ'_N	ε_{N+2}	κ_{N+2}	χ_{N+2}	κ'_{N+2}	ω	Δ^{N+2}	e_N	e_{N+2}
^{92}Sr	3	838	−32.01	0.00	−7.84	347.2	−15.00	−0.88	0.00	15	1900	1.53	1.53[a]
^{94}Sr	4	365	−50.00	0.00	75.01	451.7	−41.81	0.00	0.00	15	1800	1.16	1.53
^{96}Sr	5	620	−35.00	0.64	53.43	242.7	−20.00	−0.79	9.84	15	1500	1.33	0.86
^{98}Sr	6	526	−28.19	1.88	18.59	279.1	−34.96	−0.72	0.23	15	1360	0.78	2.22
^{100}Sr	7	526[b]	−28.19[b]	1.88[b]	18.59[b]	387.3	−43.16	−0.77	−2.99	15	1360	0.78[b]	1.93
^{102}Sr	8	526[b]	−28.19[b]	1.88[b]	18.59[b]	387.3	−46.41	−0.77	−2.99	15	1360	0.78[b]	1.93[c]

[a] $\hat{T}(E2)$ intruder parameter taken from ^{94}Sr.
[b] Hamiltonian and $\hat{T}(E2)$ parameters for the regular sector taken from ^{98}Sr.
[c] $\hat{T}(E2)$ intruder parameter taken from ^{100}Sr.

We impose as a constraint that parameters change smoothly in passing from isotope to isotope. Moreover, we try to keep as many parameters as possible at a constant value. The value of Δ^{N+2} evolves, being larger for the lightest isotopes, around $\Delta^{N+2} = 1900$ keV, but it drops down to $\Delta^{N+2} = 1360$ keV for the majority of isotopes.

The resulting values of the parameters for the IBM-CM Hamiltonian and $\hat{T}(E2)$ operator are given in Table I. In this table certain parameters could not be determined unequivocally from the experimental information. In particular, the parameters corresponding to the regular sector of $^{100-102}$Sr cannot be fixed because all known experimental states belong to the intruder sector, therefore we have assumed the same values as for ^{98}Sr. Moreover, the intruder effective charge for ^{92}Sr and ^{102}Sr are taken from ^{94}Sr and ^{100}Sr, respectively. The variation of the parameters from isotope to isotope is relatively smooth, although with some exceptions, such as the effective charge e_{N+2} in ^{96}Sr, where a sudden drop is observed, without an obvious explanation.

IV. CORRELATION ENERGY IN THE CONFIGURATION MIXING APPROACH

Intruder states are expected to appear, in principle, at much higher energies than the regular ones because a large amount of energy is needed to create a 2p-2h excitation across the shell gap. In the case of Sr, this energy gap corresponds to the proton shell closure at $Z = 40$. The energy needed to generate the excitation should be corrected by the pairing energy gain due to the formation of two extra 0^+ pairs. In our fit, this energy is $\Delta^{N+2} = 1900$ keV for ^{92}Sr and steadily drops to $\Delta^{N+2} = 1340$ keV for $^{98-102}$Sr. The former energies do not correspond to the position of the intruder bandhead due to the effect of the so-called correlation energy in both the regular and the intruder configurations. Hence, the interaction among the bosons reduces considerably the energy of the configuration; therefore, to know the relative positions of regular and intruder states, one needs to understand how this energy gain behaves. First of all, one should consider that this energy gain increases with the number of bosons, being, in principle, larger for the intruder than for the regular configuration. Moreover, it increases as one approaches the mid-shell, where its maximum is.

In the framework of the IBM-CM it is quite straightforward to analyze the correlation energy of regular and intruder configurations separately, simply switching off the mixing term between both spaces, obtaining a set of unperturbed energies. In Fig. 2, we present the value of the reference energy for the regular states, which is set by convention at 0, and for the intruder ones, which corresponds to Δ^{N+2}. The thick red dashed line represents the unperturbed energy of the regular ground state. As can be seen, there is a relatively large energy gain and it can be understood because of the large value of $|\kappa_N|$. The last two points corresponding to $^{100-102}$Sr should be considered as an extrapolation trend because the value of the regular parameters of the Hamiltonian could not be fixed due to the lack of experimental information. In the case of the intruder configuration, corresponding to the thick green dashed line, the contribution for ^{92}Sr is quite modest but it steadily increases, reaching a maximum for ^{102}Sr. The crucial point is that from ^{98}Sr onward the intruder configuration is below the regular one and the separation in energy between the two configurations increases with the neutron number.

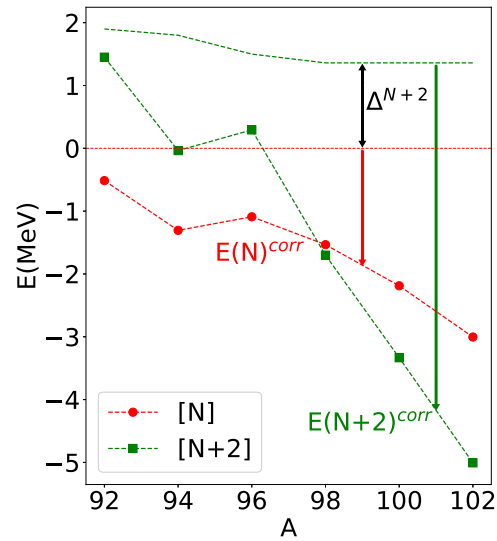

FIG. 2. Absolute energy of the lowest unperturbed regular and intruder 0^+_1 states for $^{92-102}$Sr. The arrows correspond to the correlation energies in the N and $N+2$ subspaces (see also the text for a more detailed discussion).

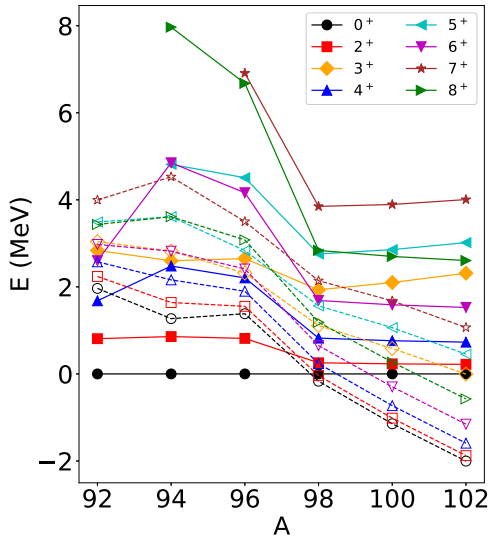

FIG. 3. Energy spectra for the IBM-CM Hamiltonian presented in Table I, switching off the mixing term. The two lowest-lying regular and intruder states for each of the angular momenta are shown (full lines with closed symbols for the regular states and dashed lines with open symbols for the intruder ones).

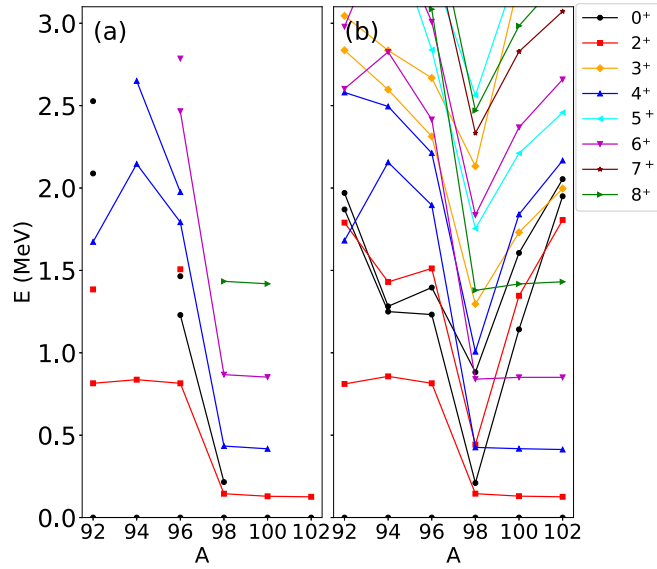

FIG. 4. Experimental excitation energies (up to $E \approx 3.0$ MeV) [panel (a)] and theoretical results [panel (b)] obtained from the IBM-CM. Only two excited states (if known experimentally) per angular momentum are plotted.

In Fig. 3, the theoretical spectra of the Sr isotopes are presented, with the mixing term fixed to zero and considering as a reference the ground state of the regular configuration. The first worthy aspect is the kink observed in the intruder spectrum for $L > 2$, with a maximum at $A = 94$ which could be related to the filling of the $d_{5/2}$ orbit, as happens in the case of Zr [34]. The regular spectrum presents a rapid change from a vibrational pattern into a rather rotational one. Note that the regular energy systematics for $A > 98$ should be regarded with certain caution because for these nuclei the same parameters as for ^{98}Sr were taken. In the case of the intruder states, the spectrum shows a quite smooth evolution from a vibrational-like spectrum into a rotational one and, at the same time, its relative position with respect to the regular bandhead is evolving, becoming the ground state of the system from $A = 98$ onward.

V. DETAILED COMPARISON FOR ENERGY SPECTRA AND $B(E2)$ TRANSITION RATES

In this section, we compare in detail the theoretical calculations with the experimental data up to an excitation energy of $E \approx 3$ MeV. In Fig. 4(a) we present the experimental excitation energies and in Fig. 4(b) the theoretical ones. Note that, for the whole chain, the theoretical 2_1^+ excitation energy closely follows the experimental one because for this level a large weight has been used in the fit procedure (see Sec. 3.2 of Ref. [60] for details). In the case of $A = 92$ and $A = 94$, the excitation energies are greatly affected by the presence of the neutron shell closure at 50 and the subshell closure at 56, which produces a kink in the excitation energy of several states, although not so abrupt as in the case of Zr isotopes. The spectrum of ^{92}Sr has a vibrational-like behavior but the energies of the two-phonon triplet members are quite scattered, while the theoretical ones appear much closer in energy. The experimental information for ^{94}Sr is quite scarce, with the noticeable absence of experimental excited 0^+ states (although in [52] a 0^+ state at 1880 keV has been observed) and the kink observed for the $4^+_{1,2}$ states, which is extended up in angular momentum in the theoretical case. Theoretically, the kink is reproduced and a low-lying excited 0^+ level is *predicted* at an energy similar to the experimental one for ^{96}Sr. This theoretical value should be regarded with caution because the calculation has been constrained to get a spectrum consistent with the neighbor nuclei. For ^{96}Sr, the agreement between theory and experiment is good, except for the states 4_2^+ and 6_2^+ which are predicted too high in energy. In the case of ^{98}Sr, the abrupt change in the structure of the spectrum is perfectly reproduced with a rather rotational spectrum for the yrast band and a very low first excited 0^+ state. For $^{100-102}$Sr very few experimental levels are known and the theoretical spectra correspond to a rotational yrast band and to a intruder configuration whose energy increases as one moves away from the neutron number 60.

The experimental information about $B(E2)$ transition rates is scarce and only a few values are known. In Table II, the known experimental values and the theoretical ones are compared in a detailed way and, moreover, in Figs. 5 and 6 intra- and interband transitions are depicted, respectively. The agreement between theory and experiment is satisfactory and no noticeable disagreements exist. The appropriate reproduction of the transition rates is a quite stringent test for the model, therefore the obtained agreement proves that the presented calculations are reliable enough, especially for ^{96}Sr and ^{98}Sr where the experimental information is more abundant.

In Fig. 5, the intraband $B(E2)$ reduced transition probabilities for the yrast band are drawn. The observed trend shows a

TABLE II. Comparison of the experimental absolute $B(E2)$ values (given in W.u.) with the IBM-CM Hamiltonian results. Data are taken from the Nuclear Data Sheets [35–42], complemented with references presented in Sec. II.

Isotope	Transition	Experiment	IBM-CM
^{92}Sr	$2_1^+ \to 0_1^+$	8(3)	8
	$2_2^+ \to 0_1^+$	0.35(18)	0.00
	$2_3^+ \to 2_1^+$	>1.2	0.04
	$0_3^+ \to 2_1^+$	0.25(17)	0.28
^{94}Sr	$2_1^+ \to 0_1^+$	8(4)	8
	$4_1^+ \to 2_1^+$	1.2(2)[a]	1.2
^{96}Sr	$2_1^+ \to 0_1^+$	13(8)	13
	$0_2^+ \to 2_1^+$	15.3(16)	9.90
	$0_3^+ \to 2_1^+$	0.028(11)	0.027
	$2_2^+ \to 2_1^+$	>8.9	8.6
	$4_1^+ \to 2_1^+$	$3(^{+8}_{-2})$[a]	1
^{98}Sr	$2_1^+ \to 0_1^+$	96(3)	96
	$0_2^+ \to 2_1^+$	$62(^{+7}_{-6})$	46
	$4_1^+ \to 2_1^+$	$124(^{+10}_{-9})$	147
	$6_1^+ \to 4_1^+$	174.8(18)	156.9
	$2_2^+ \to 4_1^+$	<12	2.6
	$2_2^+ \to 0_2^+$	$13(^{+5}_{-4})$	13
	$2_2^+ \to 0_1^+$	$0.8\ (^{+5}_{-3})$	0.02
	$8_1^+ \to 6_1^+$	$122(^{+25}_{-18})$	152
	$10_1^+ \to 8_1^+$	$126(^{+25}_{-18})$	136
	$6_2^+ \to 4_1^+$	$0.00010(^{+4}_{-3})$	0.00022
^{100}Sr	$2_1^+ \to 0_1^+$	103 (5)	103

[a]Data taken from Ref. [47].

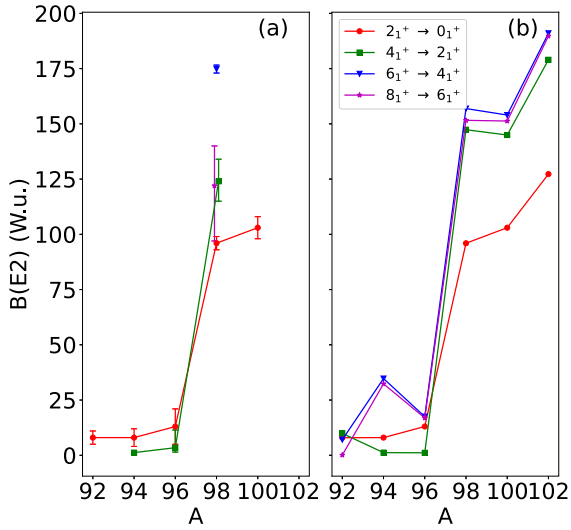

FIG. 5. Comparison of the absolute $B(E2)$ transition probabilities along the yrast band, given in W.u. Panel (a) corresponds to known experimental data and panel (b) to the theoretical IBM-CM results.

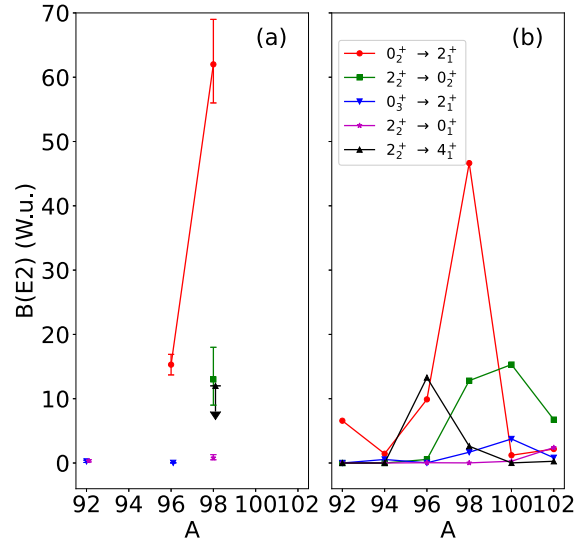

FIG. 6. Comparison of the few non-yrast intraband absolute $B(E2)$ transition probabilities, given in W.u. Panel (a) corresponds to the known experimental data, panel (b) to the theoretical IBM-CM results. The arrow for $A = 98$ represents an upper limit.

clear increase in the collectivity as the mass number increases, with an abrupt change when passing from $A = 96$ to $A = 98$, and showing the influence of the $d_{5/2}$ filling in the peak that appears for theoretical $6_1^+ \to 4_1^+$ and $8_1^+ \to 6_1^+$ transitions. In Fig. 6, the interband transitions are depicted. One can see a rather flat behavior for the major part of the transitions, except for $0_2^+ \to 2_1^+$ and $2_2^+ \to 4_1^+$ which present a peak around $A = 98$, where the abrupt change in the nuclear structure of Sr isotopes is known to exist. The transition $2_2^+ \to 0_2^+$ shows a sudden increase from $A = 98$ onward.

In Figs. 7 and 8, the detailed experimental spectra up to an excitation energy $E \approx 3$ MeV and $B(E2)$ transition rates are presented, corresponding to experimental values and theoretical results, respectively. The separation of bands was carried out first, considering an yrast band and then grouping the rest of the levels around a 0^+ or 2^+ bandhead. ^{92}Sr presents a clear vibrational structure with the two-phonon state placed at double the energy of the single-phonon state, although the energies of the triplet members are quite split, with a very low $B(E2; 2_2^+ \to 0_1^+)$ value connecting the two and the zero phonon states. The rest of states could be identified with intruder states. In the case of ^{94}Sr, it is hard to disentangle its structure because only three excited states below $E_x = 3$ MeV are known; moreover, the fact that $B(E2; 2_1^+ \to 0_1^+) \gg B(E2; 4_1^+ \to 2_1^+)$ and that $E(4_1^+) \gg E(2_1^+)$ hinders the identification as a vibrational nucleus. The theoretical calculation suggests that the 4_1^+ state has an intruder nature and it also generates two low-lying 0^+ states, not know experimentally: one intruder and the other of regular nature. ^{96}Sr apparently presents a vibrational-like structure but with already a large influence of the intruder states as shown in the departure from the vibrational case of the $B(E2)$ values connecting double and single phonon states. Moreover, the existence of several low-lying 0^+ states points towards the presence of intruder states. In ^{98}Sr the yrast band already presents

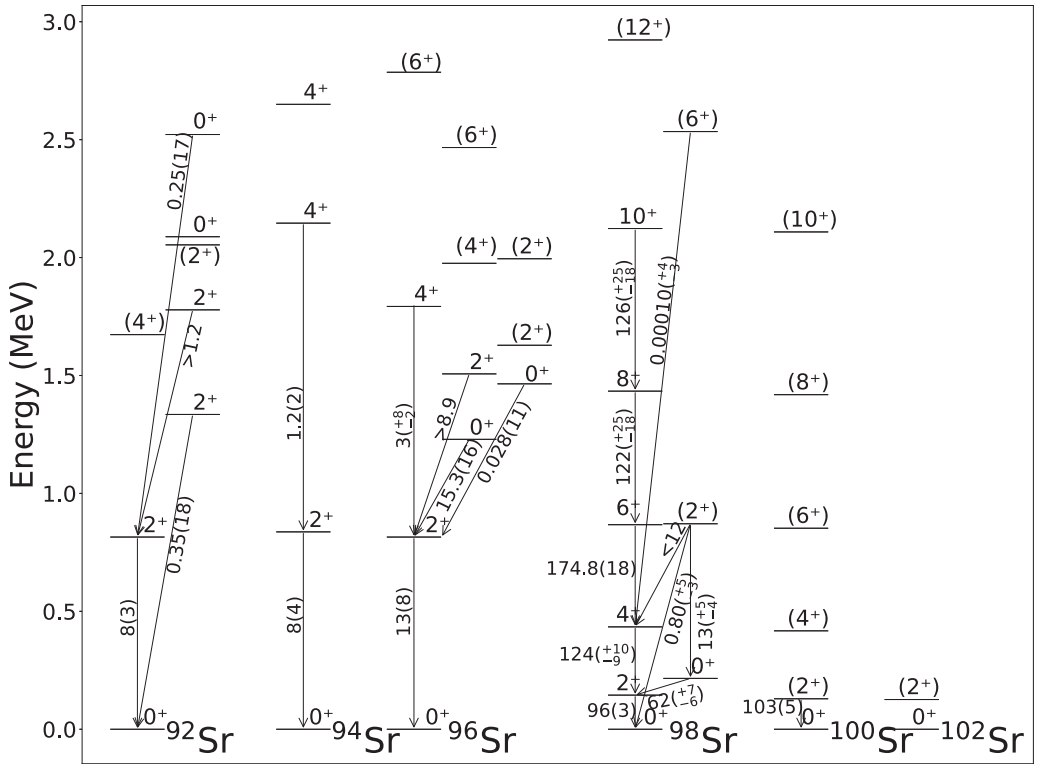

FIG. 7. Experimental excitation energies and absolute $B(E2)$ transition rates (given in W.u.) for selected states in $^{92-102}$Sr.

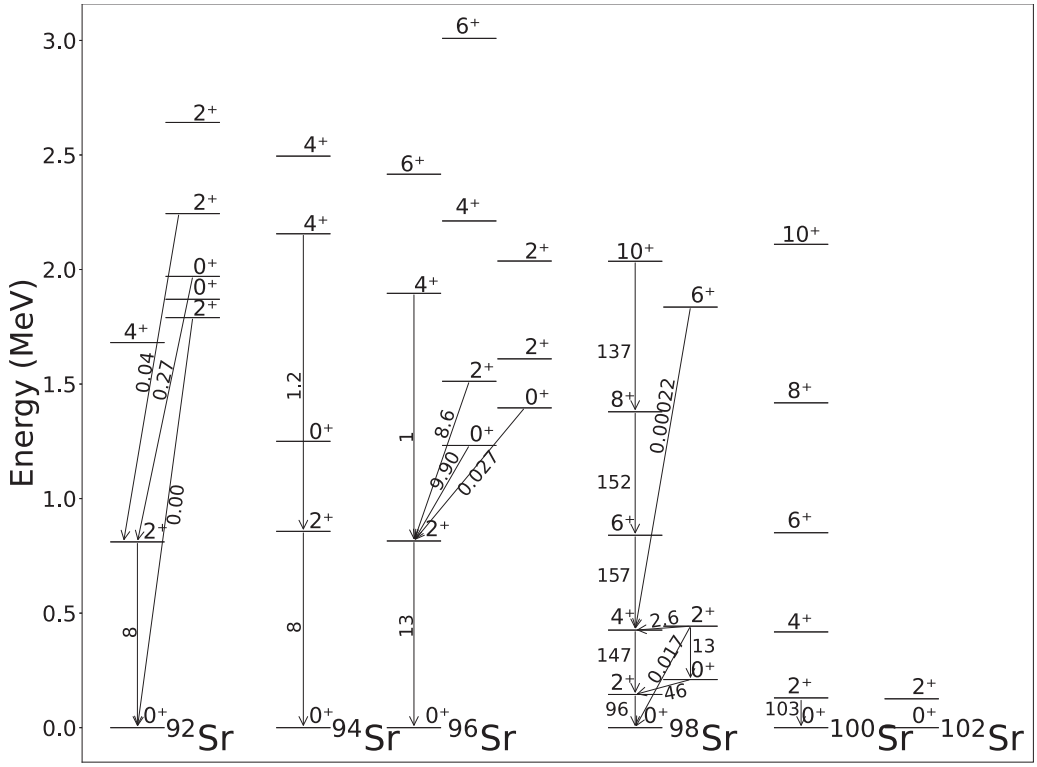

FIG. 8. Theoretical excitation energies and absolute $B(E2)$ transition rates (given in W.u.) for selected states in $^{92-102}$Sr.

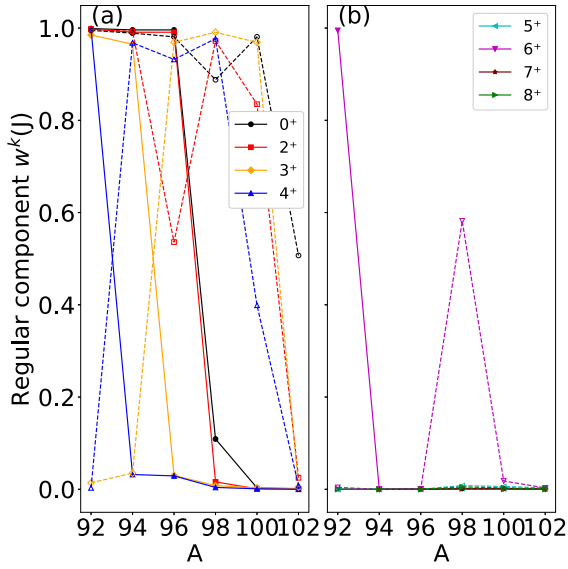

FIG. 9. Regular content of the two lowest-lying states for each J value (full lines with closed symbols correspond to the first state while dashed lines with open symbols correspond to the second state) resulting from the IBM-CM calculation.

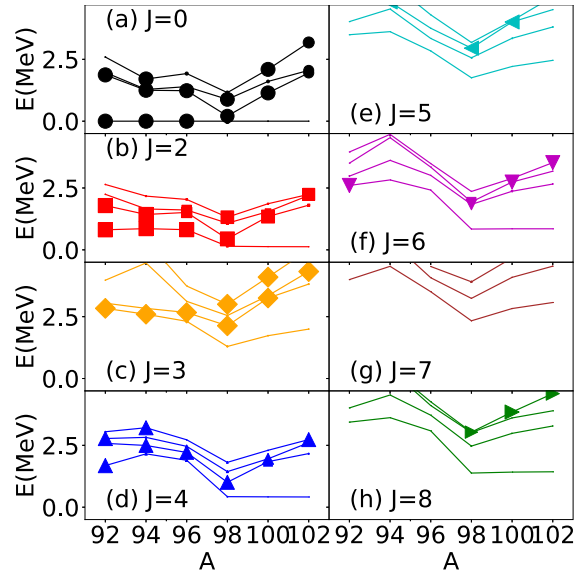

FIG. 10. Energy systematics of the four lowest states below 4 MeV. The size of the symbol is proportional to the value of $w^k(J)$ (see text for details). Each panel corresponds to a given angular momentum: (a) $J = 0$, (b) $J = 2$, (c) $J = 3$, (d) $J = 4$, (e) $J = 5$, (f) $J = 6$, (g) $J = 7$, and (h) $J = 8$.

a rotational spacing because the first 0^+ intruder state becomes the ground state. Concerning the $B(E2)$ values, they present a certain departure from the rotational case for the highest angular momenta. The 0_2^+ state is the bandhead of the regular band and the observed $B(E2)$ values associated with this band show a clear correspondence with the case of ^{96}Sr, namely, $B(E2; 2_2^+ \to 0_2^+) = 13$ W.u. in ^{98}Sr while $B(E2; 2_1^+ \to 0_1^+) = 13$ W.u. in ^{96}Sr too, suggesting the crossing of the regular and the intruder bands. Finally, for ^{100}Sr a clear rotational yrast band is observed and for ^{102}Sr only the state 2_1^+ is known experimentally.

VI. WAVE FUNCTION STRUCTURE: CONFIGURATION MIXING AND UNPERTURBED STRUCTURE

To disentangle the structure of the states, the first step is to calculate the fraction of the wave function lying in the sectors $[N]$ and $[N + 2]$. Figure 9 shows the fraction of the wave function within the regular sector, $[N]$, defined as $w^k(J) \equiv \sum_i |a_i^k(J)|^2$ (the a's being the coefficients of the wave function in the regular sector and k an index), for the first two members of each angular momentum (full line for the first and dashed for the second state). The ground state experiences a rapid transition from an almost regular structure, up to $A = 96$, into a fully intruder one from $A = 98$ onward. The same trend is observed for the 2_1^+, 3_1^+, 4_1^+, and 6_1^+ states, but in this case the transitions appear at $A = 98$, $A = 96$, $A = 94$, and $A = 94$, respectively, while for the 5_1^+, 7_1^+, and 8_1^+ states an intruder structure is shown for all values. For the second member of the angular momenta (dashed line), in the case of 5_2^+, 7_2^+, and 8_2^+, the states are of intruder nature all the way; the 0_2^+ state has a regular structure except for $A = 102$; the 2_2^+ state is strongly mixed at $A = 96$, and it is mainly of regular character for $A = 92, 94, 98$, and 100 and of intruder nature for $A = 102$; the state 3_2^+ presents regular character for $A = 96, 98$, and 100 and intruder for $A = 92, 94$, and 102; the 4_2^+ state presents regular character for $A = 94, 96$ and 98, intruder for $A = 92$ and 102, and is mixed for $A = 100$; finally the 6_2^+ state is regular for $A = 92$, mixed for $A = 98$, and intruder for the rest of the isotopes.

The results on the regular content of the wave function that we have presented, so far, in Fig. 9 are strongly influenced by the crossing of the different levels and, therefore, they could mask a smooth trend. To overcome this problem, we present the regular content of the first four states per angular momentum in the same plot as the excitation energy of the states, making the size of the dot associated with each state proportional to the regular content of the wave function. In Fig. 10 we present such information, calibrating the size of the dot for the 0_1^+ state of $A = 92$ to regular content of 100%. For the states 0^+, 2^+, 3^+, and 4^+ one can see how the regular content "moves" from one to another state, depending on the way the levels cross; however for angular momenta 5^+, 6^+, 7^+, and 8^+ the majority of the states show a intruder character and, therefore, the regular states should appear at much higher energy, not shown in the figure.

A different decomposition of the wave function that provides extra information is obtained by first calculating the wave functions within the $[N]$, $|l, JM\rangle_N$, and $[N + 2]$ subspace, $|m, JM\rangle_{N+2}$, defining an "intermediate" basis [66,67] that corresponds to the states appearing in Fig. 3, where the mixing term, ω, has been canceled. This generates a set of unperturbed bands within the 0p-0h and 2p-2h subspaces.

The overlaps squared, $|_N\langle l, JM \mid k, JM\rangle|^2$ and $|_{N+2}\langle m, JM \mid k, JM\rangle|^2$, are depicted in Fig. 11 for $k = 1, 2$, $(l, m) = 1, 2, 3$, and $J^\pi = 0^+, 2^+, 3^+, 4^+, 5^+, 6^+, 7^+, 8^+$. This way of presenting the wave function shows in a very

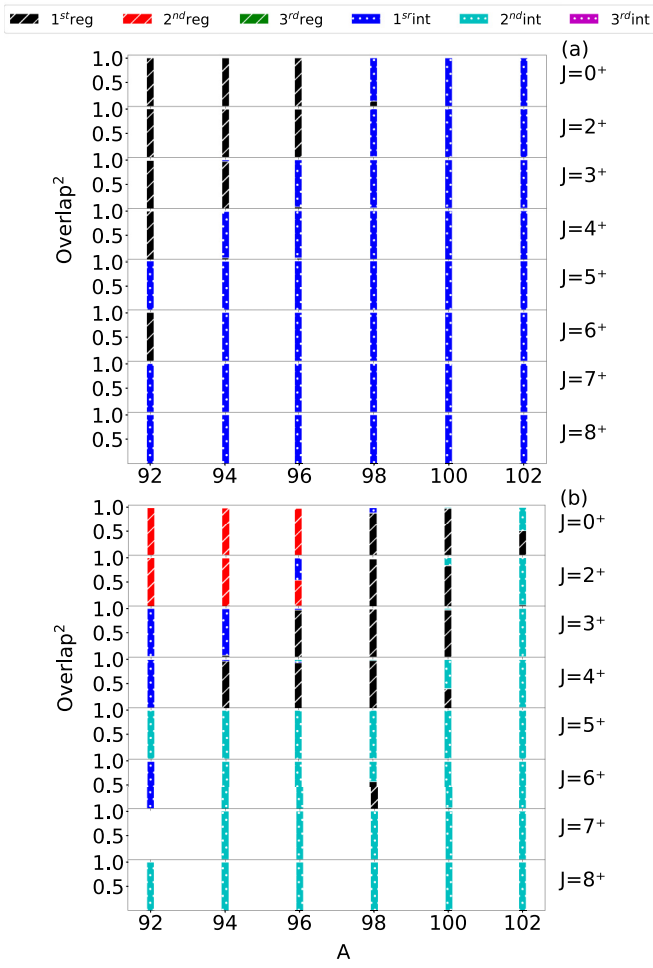

FIG. 11. Overlap of the wave functions with the wave functions describing the unperturbed basis. (a) Overlaps for the first $0^+, 2^+, 3^+, 4^+, 5^+, 6^+, 7^+, 8^+$ states ($k = 1$). (b) Overlaps for the corresponding second state ($k = 2$) (see also text).

visual form how the structure of the states evolves along the isotope chain. Regarding the first members of the different angular momenta, for the 0^+ and 2^+ states, they correspond to the first regular state, from $A = 92$ up to $A = 96$, but suddenly change to the first intruder one in the range $A = 98$–102; in the case of 3^+, the first two isotopes correspond to the first regular state while the rest correspond to the first intruder one; for 4^+ and 6^+, only $A = 92$ fully overlaps with the first regular state and the rest of the isotopes overlap with the first intruder one; finally, for 5^+, 7^+ and 8^+, all the states present a complete overlap with the first intruder state. Therefore, the first members of the different angular momenta have a very pure structure without noticeable mixing, presenting a sudden transition when passing from $A = 96$ to $A = 98$, but moving to lower atomic mass values as J increases. For the second members the reality is much more involved, the 0^+ state having a complete overlap with the second regular member for $A = 92$–96, with the first regular state for $A = 98$–100, and a mixture of the first regular and the second intruder states for $A = 102$; the state 2^+ for $A = 92$–94 has a full overlap with the second regular state, for $A = 96$ it is a mixture of the second regular and the first intruder states, for $A = 98$–100 it overlaps with the first regular state, and for $A = 102$ it overlaps with the second intruder one; 3^+ is a rather pure state corresponding to the first intruder, first regular and second intruder members for $A = 92$–94, $A = 96$–100, and $A = 102$, respectively; 4^+ is also rather pure except for $A = 100$ where a mixture between the first regular and the second intruder states exits, having for $A = 92$, $A = 94$–98, and $A = 102$ a complete overlap with the first intruder, the first regular, and the second intruder states, respectively; for 5^+, 6^+, 7^+, and 8^+, in most of the cases, there is a full overlap with the second intruder state but with some exceptions.

VII. STUDY OF OTHER OBSERVABLES: RADII, ISOTOPIC SHIFTS, AND TWO-NEUTRON SEPARATION ENERGIES

A. Radii and isotopic shifts

Nuclear radius is an experimental observable that provides a direct information on the nuclear deformation, hence it is an excellent probe to detect abrupt changes in nuclear structure, as it is expected to exist at neutron number 60. In this section we will compare the theoretical value predicted by the IBM-CM with the experimental data [68].

The value of the radius of a nucleus calculated with the IBM is encoded in the matrix element of the $\hat{n}_d$ operator for the ground state. This value should be superimposed to a linear trend that depends on the number of bosons. Moreover, in the case of the IBM-CM one also needs to consider both the regular and the intruder configurations. In summary, the radius can be expressed as

$$r^2 = r_c^2 + \hat{P}_N^\dagger(\gamma_N \hat{N} + \beta_N \hat{n}_d)\hat{P}_N + \hat{P}_{N+2}^\dagger(\gamma_{N+2}\hat{N} + \beta_{N+2}\hat{n}_d)\hat{P}_{N+2}, \quad (5)$$

where $\hat{P}$ are projection operators, the appearing parameters are common for the whole chain of isotopes, and they are fixed to reproduce as well as possible the experimental data, which refer to ^{88}Sr. r_c^2 is chosen to match the radius of ^{92}Sr. The resulting values are $\gamma_N = 0.23$ fm^2, $\beta_N = -0.028$ fm^2, $\gamma_{N+2} = 0.294$ fm^2, and $\beta_{N+2} = -0.16$ fm^2. A similar approach is conducted in [69] but only considering a single configuration.

The overall description of the radii and even of the isotope shifts is rather satisfactory, as can be readily observed in Fig. 12, reproducing nicely the sudden onset of deformation in ^{98}Sr. This feature points towards the appropriated reproduction of the crossing of two configurations with a rather different deformation which is, as a matter of fact, responsible for the abrupt increase of the nuclear radius at $A = 98$.

B. Two-neutron separation energies

The definition of the S_{2n} involves the value of the binding energy of two neighboring nuclei separated by two units of mass, written as

$$S_{2n}(A) = \mathrm{BE}(A) - \mathrm{BE}(A-2), \quad (6)$$

where BE denotes the binding energy of the nucleus. In the case of the IBM, one needs to add to the obtained binding

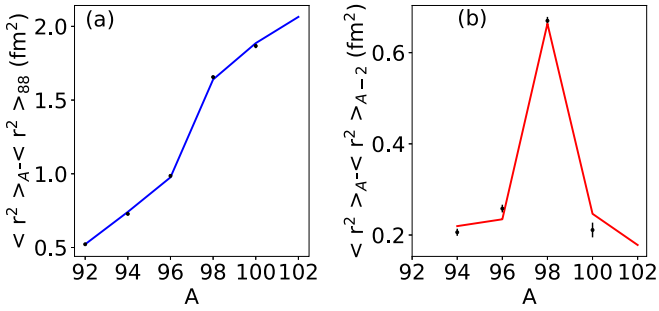

FIG. 12. (a) Charge mean-square radii for the Sr nuclei. (b) Isotopic shift for the Sr nuclei. The data are taken from [68]. Lines show theoretical results and dots with error bars are experimental values.

energy a contribution that depends on N and N^2, not affecting the excitation energies. This leads to an extra linear contribution to the value of S_{2n} [70]. Therefore, S_{2n} can be written as

$$S_{2n}(A) = \mathcal{A} + \mathcal{B}A + \mathrm{BE}^{lo}(A) - \mathrm{BE}^{lo}(A-2), \qquad (7)$$

where BE^{lo} is the local binding energy derived from the IBM Hamiltonian, and the coefficients $\mathcal{A}$ and $\mathcal{B}$ are assumed to be constant for a chain of isotopes [70]. In the case of IBM-CM calculations we expect that the effective number of bosons for the ground state can be affected by the influence of the intruder states. To consider this effect, we propose as an ansatz

$$S_{2n}(A) = \mathcal{A} + \mathcal{B}(A + 2(1-w)) + \mathrm{BE}^{lo}(A) - \mathrm{BE}^{lo}(A-1), \qquad (8)$$

where $\omega = \omega^1(0)$ $[w^k(J) \equiv \sum_i |a_i^k(J)|^2]$. The values of $\mathcal{A}$ and $\mathcal{B}$ are determined, once the BE^{lo}'s are known, through a least-squares fit to the experimental values of S_{2n}, as explained in detail in [33,62,70]. In our case, the obtained values are $\mathcal{A} = 52.9$ MeV and $\mathcal{B} = -0.441$ MeV, and in Fig. 13 the comparison between experiment and theory shows remarkably good agreement around neutron number

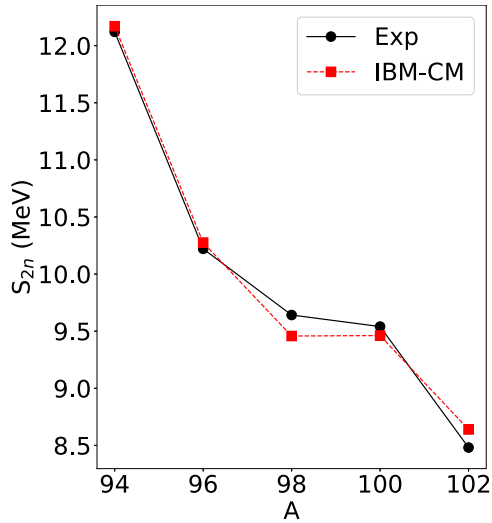

FIG. 13. Comparison of experimental and theoretical two-neutron separation energies.

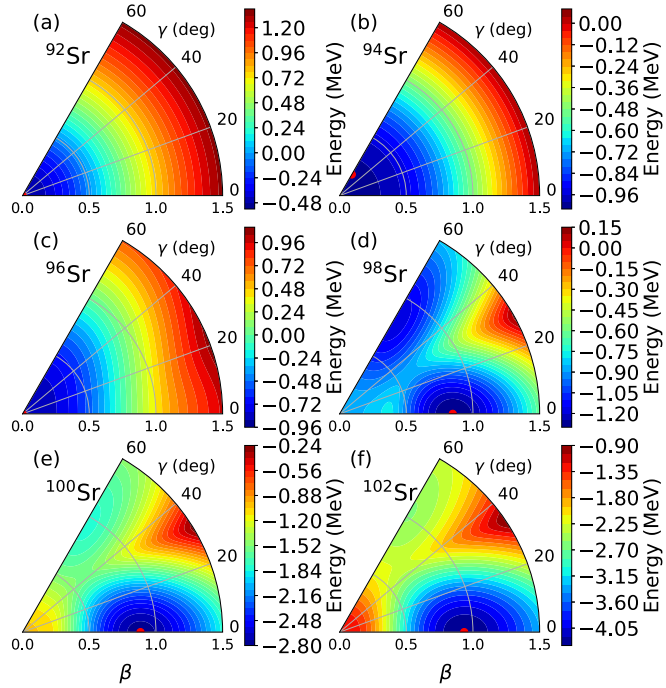

FIG. 14. Matrix coherent-state calculations for $^{92-102}$Sr, corresponding to the present IBM-CM Hamiltonian (Table I). Results are plotted in the (β, γ) plane in the range $0.0 \leqslant \beta \leqslant 1.5$ and $0^\circ \leqslant \gamma \leqslant 60^\circ$. The red dot marks the position of the absolute minimum.

60 ($A = 98$) where the flattening of the curve is more evident, corresponding to the place where regular and intruder configurations cross. This type of behavior could be identified with the onset of a quantum phase transition (QPT) [71], as already suggested for the case of Zr [34].

VIII. NUCLEAR DEFORMATION AND MEAN-FIELD ENERGY SURFACES

The goal of this section is to obtain information about the evolution of the deformation along the isotope chain, taking into account that deformation (β) is not a direct observable. The use of different methods to determine the deformation will allow us to analyze the consistency of the obtained values.

The first way to get information about deformation is through the use of the intrinsic state formalism of the IBM. This formalism was presented in the set of seminal works [72–75] and it provides a geometric interpretation of the model, defining, in particular, a deformation parameter. This intrinsic state formalism cannot be used directly for the IBM-CM, but the formalism should be enlarged. Frank *et al.* introduced almost twenty years ago the matrix coherent-state method [76–79] which allows one to calculate the total energy surface for a system where regular and intruder configurations exist. In Refs. [33,62,64,80], a detailed description of the method and its application to Pt, Hg, Po, and Zr isotopes, respectively, has been given. In Fig. 14, the IBM-CM mean-field energy surfaces are presented for the isotopes $^{92-102}$Sr. In these nuclei, one can see how the three lightest isotopes present a rather spherical shape, although with a small

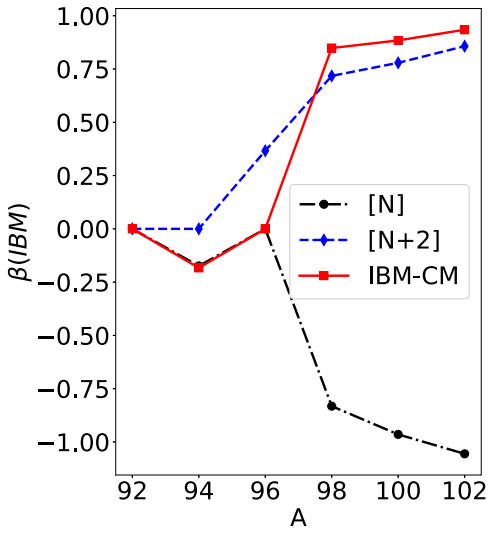

FIG. 15. Value of β extracted from the IBM-CM energy surface. $[N]$, $[N+2]$, and IBM-CM correspond to a pure regular configuration, a pure intruder configuration, and to the complete calculation.

deformation for ^{94}Sr and a rather flat well for ^{96}Sr; however, the three heaviest ones are well deformed with a prolate shape, presenting for ^{98}Sr a clear coexistence between a prolate and an oblate minima that are almost degenerate. In $^{100-102}$Sr, the nuclei present a well deformed prolate minimum coexisting with an oblate one at a higher energy. The obtained energy surfaces are in close correspondence with the ones appearing in [29,32] where a HFB calculation using a Gogny interaction is performed. In that work, ^{92}Sr is still spherical and a small oblate deformation already appears for ^{94}Sr, in ^{96}Sr an oblate and a prolate minima already coexist, the deepest minimum corresponding to the oblate shape, and the same holds for $^{98-102}$Sr, but in these cases the prolate minimum is the deepest one. It is worthwhile to mention that in Zr isotopes a quite similar situation exists but with the coexistence of a spherical and a prolate minima (at the IBM-CM energy surface), and oblate and prolate minima in the case of Sr.

To better illustrate the coexistence of two different shapes, in Fig. 15 we depict the value of β corresponding to the absolute minimum resulting from the present IBM calculation. Note that this IBM β variable is not equivalent to the one of the collective model but can be approximately connected as explained in [72]. On the one hand, we present the values for the regular and the intruder sectors separately, labeled with $[N]$ and $[N+2]$, respectively, assuming that no interaction exits between them, imposing $\omega = 0$, and, on the other hand, we present the value of β obtained from the full calculation, IBM-CM. In this figure, it is readily appreciated how both configurations are evolving from an almost spherical shape into an oblate ($[N]$) or a prolate one ($[N+2]$), the onset of deformation being a little more abrupt in the case of the regular configuration than in the intruder case. The complete calculation shows how the first three isotopes correspond to the regular configuration (spherical) while the last three isotopes correspond to the intruder one (prolate).

Even though the shape of a certain nucleus is not an observable, the study of Coulomb excitation allows us to extract, in an almost model independent way, information about nuclear deformation, as shown by Kumar, Cline, and coworkers [81,82]. This approach is based on the use of the concept of "equivalent ellipsoid" of a given nucleus, corresponding to an ellipsoid defined as uniformly charged with the same charge, $\langle r^2 \rangle$, and $E2$ moments as the original nucleus characterized by a specific eigenstate. Starting from measured data on various transitions using Coulomb excitation methods, it turns out that the data allow one to extract for a given state with defined angular momentum an extra set of two numbers that fit with the variables of the collective model, β and γ. More recently, in Refs. [83–85] the authors have addressed the question of nuclear deformation within the laboratory frame, even extending toward excited states making use of the auxiliary-field Monte Carlo method.

In order to obtain, from a theoretical point of view, the nuclear shape, we will make use of the quadrupole shape invariants. Hence, the quadrupole deformation for the 0^+ states corresponds to

$$q_{2,i} = \sqrt{5}\langle 0_i^+ | [\hat{Q} \times \hat{Q}]^{(0)} | 0_i^+ \rangle, \tag{9}$$

$$q_{3,i} = -\sqrt{\frac{35}{2}}\langle 0_i^+ \mid [\hat{Q} \times \hat{Q} \times \hat{Q}]^{(0)} \mid 0_i^+ \rangle. \tag{10}$$

The deformation parameters are directly connected with the ones of the triaxial rigid rotor, q and δ, according to

$$q = \sqrt{q_2}, \tag{11}$$

$$\delta = \frac{60}{\pi} \arccos \frac{q_3}{q_2^{3/2}}, \tag{12}$$

where δ coincides with the parameter γ of the Bohr-Mottelson model up to first-order approximation. It is worthwhile mentioning the work [86], where a method to calculate the fluctuations of β and γ is presented.

The theoretical values of γ and q^2 are presented in Table III simultaneously with the fraction of wave function belonging to the regular sector w^k, for every 0_1^+, 0_2^+, and 0_3^+ of the whole chain of Sr isotopes. According to this table, one readily observe the coexistence of different deformations; typically regular states are less deformed than the intruder states. Another notable feature is the fact that the deformation of the ground state suddenly increases when passing from $^{92-96}$Sr to $^{98-102}$Sr. Concerning triaxiallity, the three first isotopes present clear triaxial shapes, while in the three last ones the ground state is close to a prolate shape and the rest of states are rather triaxial.

The deformation parameter β can also be obtained from the quadrupole shape invariant (9) (see, e.g., references [87–89]),

$$\beta = \frac{4\pi\sqrt{q_2}}{3Zer_0^2A^{2/3}}, \tag{13}$$

where e is the proton charge and $r_0 = 1.2$ fm.

The values of β extracted from Eq. (13) for the corresponding ground state, 0_1^+, and the 0_2^+ and 0_3^+ states, are shown in Fig. 16(a), where β for the ground state presents a rapid increase, passing from a value around 0.15 for $^{92-96}$Sr

TABLE III. Values of deformation, q^2 and γ, extracted from the quadrupole shape invariants, together with the value of w^k ([N] content).

A	State	q^2 (e^2b^2)	γ	w^k
92	0_1^+	0.10	29	0.999
	0_2^+	0.06	17	0.995
	0_3^+	1.18	19	0.003
94	0_1^+	0.10	30	0.996
	0_2^+	0.05	30	0.989
	0_3^+	0.32	30	0.013
96	0_1^+	0.17	39	0.996
	0_2^+	0.14	49	0.981
	0_3^+	0.16	15	0.020
98	0_1^+	1.33	10	0.109
	0_2^+	0.31	15	0.888
	0_3^+	0.14	27	0.947
100	0_1	1.46	10	0.109
	0_2^+	0.25	48	0.981
	0_3^+	0.98	18	0.039
102	0_1^+	1.84	9	0.001
	0_2^+	0.81	19	0.507
	0_3^+	0.83	18	0.493

to around 0.45 for $^{98-102}$Sr. The value of β for the 0_2^+ state steadily increase while for the 0_3^+ state there also exists a sudden increase for $^{100-102}$Sr. It is very enlightening to present the value of the deformation for the first 0^+ state belonging to the regular sector, 0_{reg}^+, and the one of the first 0^+ state which belongs to the intruder sector, 0_{int}^+, as shown in Fig. 16(b), which is done simply taking into account the regular content of the states presented in the last column of Table III. The 0_{reg}^+ state shows a smooth increase of deformation over the whole chain of isotopes and it corresponds to the 0_1^+ state for $^{92-96}$Sr and to the 0_2^+ for $^{98-102}$Sr, while the state 0_{int}^+ shows the sudden increase of the deformation previously explained and

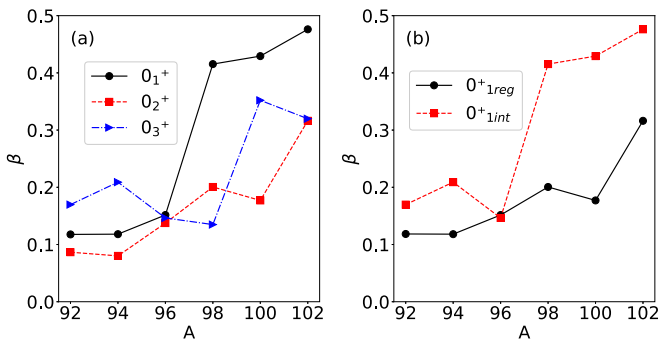

FIG. 16. Value of the deformation, β, extracted from the value of the quadrupole shape invariants. In (a) we plot the value for the first three 0^+ states. In (b) we plot the same but for the first regular and the first intruder 0^+ states (see text).

it corresponds to the states 0_3^+ and 0_1^+ for $^{92-96}$Sr and $^{98-102}$Sr, respectively.

To conclude this section, we can say that both approaches presented in this section provide a consistent view of the deformation of the two families of states, intruder and regular, with both configurations close to a spherical shape in $^{92-96}$Sr and increasing in deformation when entering in the region of $^{98-102}$Sr. The mean-field energy surfaces point to the coexistence of a prolate and an oblate shape in $^{98-102}$Sr, corresponding to the deepest minimum to the prolate shape. The abrupt onset of deformation, specially for the ground state, which is the result of the crossing of the regular and the intruder configurations, points to the existence of a QPT around ^{98}Sr. The behavior of S_{2n} and the nuclear radii, presented in previous section, point to the existence of a QPT, as well. This is a case that resembles the situation in even-even Zr isotopes where also two configurations coexist and they cross at ^{100}Zr. Therefore, the study of both chains of isotopes suggests the presence of a first-order QPT at neutron number 60 associated with the crossing of two configurations.

IX. CONCLUSIONS AND OUTLOOK

In this work we have conducted an IBM-CM calculation for the even-even $^{92-102}$Sr isotopes. The parameters of the Hamiltonian have been fixed through a least-squares procedure to the excitation energies of states below 3 MeV and to the corresponding $B(E2)$ values. The number of known experimental $B(E2)$ values, and even the number of experimental excitation energies in some cases, is quite reduced in most of the isotopes. This fact makes it impossible to fit certain parameters in some isotopes and in this situation the parameters are taken from the neighboring isotopes. Once the parameters have been determined, experimental data and theoretical values are compared, showing a more than reasonable agreement, reproducing the rapid changes observed around $A = 98$, where the systematics of the density of energy levels suddenly increase and the $B(E2)$ values rapidly increase, as well. The calculation of unperturbed bands, without the mixing term, clearly shows the crossing of two families of states with a much larger gain of correlation energy in the case of the intruder configuration from ^{98}Sr onward. The wave functions have been also studied in detail, clearly showing abrupt changes around $A = 98$, the low-lying states passing from being mostly of regular character to being of intruder nature. The two-neutron separation energies and the value of the radii have been computed and compared with the experimental information, presenting a rather good agreement, reproducing the rapid changes that characterize the nuclei around ^{98}Sr. This agreement is specially relevant because the structure of the states is fixed from the Hamiltonian parameters and, therefore, the correct reproduction of this experimental information points towards a reasonable description of the wave functions. Finally, the mean-field energy surfaces and the value of the deformation have been obtained and a remarkable agreement with previous mean-field calculations is observed.

The analysis of Sr isotopes complements the previous works carried out for Zr isotopes [33,34], where a more detailed data basis has been available. The obtained results for

both families of isotopes draw a common landscape where two families of regular and intruder states cross around neutron number 60, inducing characteristic features, such as the lowering of 0^+ states, the compression of the spectrum, the enhancement of $E2$ transition rates, the flattening of the two-neutron separation energy, or the sudden increase of the nuclear radius. One can consider the later features as hints of the onset of deformation that in our case is generated by the crossing of two configurations with different degrees of deformation.

The obtained regular and intruder configurations in Sr isotopes present a reduced interaction between them, which is at the origin of the observed abrupt changes. There are other isotope chains where regular and intruder configurations also cross for the ground state, as in Pt and Po, but in these cases the interaction between both families of states is so large that all abrupt changes have been smoothed out; however, when the unperturbed configurations are studied, the results are very similar to those obtained in this work.

Further experimental information for Sr isotopes will allow us to better determine some of the parameters of the Hamiltonian and the $E2$ transition operator. As an outlook, we hope that from the experimental side effort is enhanced to expand the present data basis with measurements of excitation energies and both $E2$ and $E0$ transition rates which are well known to give essential information on the variation of shape associated with the connected states. One has at this moment good hints of changing deformation of the ground state structure, but more data, preferentially leading to complementary information, are needed for the Sr isotopes to extend the experimental knowledge beyond $N = 100$ and further. Spectroscopy using fission at and near nuclear reactors and separation of the fission products, which has been already carried out for the Zr isotopes, are highly demanded for Sr isotopes too.

ACKNOWLEDGMENTS

We are very grateful to K. Heyde for the careful reading of this manuscript. This work was supported by the Grant No. PID2019-104002GB-C21 funded by MCIN/AEI/10.13039/501100011033 and FEDER "A way of making Europe," the Consejería de Economía, Innovación, Ciencia y Empleo de la Junta de Andalucía (Spain) under Group FQM-370, and by FEDER SOMM17/6105/UGR. Resources supporting this work were provided by the CEAFMC and the Universidad de Huelva High Performance Computer (HPC@UHU) funded by ERDF/MINECO Project No. UNHU-15CE-2848.

[1] T. Otsuka, Y. Tsunoda, T. Togashi, N. Shimizu, and T. Abe, Single-particle states vs. collective modes: Friends or enemies? EPJ Web Conf. **178**, 02003 (2018).

[2] H. Morinaga, Interpretation of some of the excited states of $4n$ self-conjugate nuclei, Phys. Rev. **101**, 254 (1956).

[3] G. E. Brown, Nuclear structure and models (ground state and low excited levels): Light nuclei C. R. Phys. **1**, 129 (1964).

[4] G. E. Brown and A. M. Green, Even parity states of ^{16}O and ^{17}O, Nucl. Phys. **75**, 401 (1966).

[5] G. E. Brown and A. M. Green, Nuclear coexistence in the oxygen region and realistic nucleon-nucleon forces, Nucl. Phys. **85**, 87 (1966).

[6] E. Caurier, J. Menéndez, F. Nowacki, and A. Poves, Coexistence of spherical states with deformed and superdeformed bands in doubly magic ^{40}Ca: A shell-model challenge, Phys. Rev. C **75**, 054317 (2007).

[7] A. Poves, Shape coexistence: The shell model view, J. Phys. G: Nucl. Part. Phys. **43**, 024010 (2016).

[8] A. Poves, Shape coexistence and islands of inversion monopole vs multipole, in *Proceedings of the IIRC Symposium on Perspectives of the Physics of Nuclear Structure, Tokyo, Japan, November 1–4, 2017* [JPS Conf. Proc. **23**, 012015 (2018)].

[9] K. Heyde, P. Van Isacker, M. Waroquier, J. L. Wood, and R. A. Meyer, Coexistence in odd-mass nuclei, Phys. Rep. **102**, 291 (1983).

[10] J. L. Wood, K. Heyde, W. Nazarewicz, M. Huyse, and P. van Duppen, Coexistence in even-mass nuclei, Phys. Rep. **215**, 101 (1992).

[11] K. Heyde and J. L. Wood, Shape coexistence in atomic nuclei, Rev. Mod. Phys. **83**, 1467 (2011).

[12] B. A. Brown and W. A. Richter, New "USD" Hamiltonians for the *sd* shell, Phys. Rev. C **74**, 034315 (2006).

[13] F. Nowacki and A. Poves, New effective interaction for $0\hbar\omega$ shell-model calculations in the *sd*-*pf* valence space, Phys. Rev. C **79**, 014310 (2009).

[14] P. Federman and S. Pittel, Towards a unified microscopic description of nuclear deformation, Phys. Lett. B **69**, 385 (1977).

[15] P. Federman, S. Pittel, and R. Campos, Microscopic study of the shape transition in the zirconium isotopes, Phys. Lett. B **82**, 9 (1979).

[16] P. Federman and S. Pittel, Unified shell-model description of nuclear deformation, Phys. Rev. C **20**, 820 (1979).

[17] P. Federman, S. Pittel, and A. Etchegoyen, Quenching of the $2p_{1/2}$-$2p_{3/2}$ proton spin-orbit splitting in the Sr-Zr region, Phys. Lett. B **140**, 269 (1984).

[18] K. Heyde, E. D. Kirchuk, and P. Federman, Coexistence or strong-mixing of intruder 0^+ states in even-even Zr nuclei, Phys. Rev. C **38**, 984 (1988).

[19] A. Etchegoyen, P. Federman, and E. G. Vergini, Importance of the neutron-proton interaction for Zr isotopes, Phys. Rev. C **39**, 1130 (1989).

[20] S. Pittel, P. Federman, G. E. Arenas Peris, R. F. Casten, and W.-T. Chou, Semiempirical determination of effective *p*-*n* monopole matrix elements, Phys. Rev. C **48**, 1050 (1993).

[21] A. Holt, T. Engeland, M. Hjorth-Jensen, and E. Osnes, Application of realistic effective interactions to the structure of the Zr isotopes, Phys. Rev. C **61**, 064318 (2000).

[22] K. Sieja, F. Nowacki, K. Langanke, and G. Martínez-Pinedo, Shell model description of zirconium isotopes, Phys. Rev. C **79**, 064310 (2009).

[23] T. Otsuka, M. Honma, T. Mizusaki, N. Shimizu, and Y. Utsuno, Monte Carlo shell model for atomic nuclei, Prog. Part. Nucl. Phys. **47**, 319 (2001).

[24] N. Shimizu, T. Abe, Y. Tsunoda, Y. Utsuno, T. Yoshida, T. Mizusaki, M. Honma, and T. Otsuka, New-generation Monte

Carlo shell model for the K computer era, Prog. Theor. Exp. Phys. **2012**, 01A205 (2012).
[25] N. Shimizu, T. Abe, M. Honma, T. Otsuka, T. Togashi, Y. Tsunoda, Y. Utsuno, and T. Yoshida, Monte Carlo shell model studies with massively parallel supercomputers, Phys. Scr. **92**, 063001 (2017).
[26] T. Togashi, Y. Tsunoda, T. Otsuka, and N. Shimizu, Quantum Phase Transition in the Shape of Zr isotopes, Phys. Rev. Lett. **117**, 172502 (2016).
[27] H. Mei, J. Xiang, J. M. Yao, Z. P. Li, and J. Meng, Rapid structural change in low-lying states of neutron-rich Sr and Zr isotopes, Phys. Rev. C **85**, 034321 (2012).
[28] J. Xiang, Z. P. Li, Z. X. Li, J. M. Yao, and J. Meng, Covariant description of shape evolution and shape coexistence in neutron-rich nuclei at N ≈ 60, Nucl. Phys. A **873**, 1 (2012).
[29] K. Nomura, R. Rodríguez-Guzmán, and L. M. Robledo, Structural evolution in $A \approx 100$ nuclei within the mapped interacting boson model based on the Gogny energy density functional, Phys. Rev. C **94**, 044314 (2016).
[30] J. P. Delaroche, M. Girod, J. Libert, H. Goutte, S. Hilaire, S. Péru, N. Pillet, and G. F. Bertsch, Structure of even-even nuclei using a mapped collective Hamiltonian and the D1S Gogny interaction, Phys. Rev. C **81**, 014303 (2010).
[31] N. Paul, A. Corsi, A. Obertelli, P. Doornenbal, G. Authelet, H. Baba, B. Bally, M. Bender, D. Calvet, F. Château, S. Chen, J.-P. Delaroche, A. Delbart, J.-M. Gheller, A. Giganon, A. Gillibert, M. Girod, P.-H. Heenen, V. Lapoux, J. Libert *et al.*, Are There Signatures of Harmonic Oscillator Shells Far from Stability? First Spectroscopy of ^{110}Zr, Phys. Rev. Lett. **118**, 032501 (2017).
[32] R. Rodríguez-Guzmán, P. Sarriguren, L. M. Robledo, and S. Perez-Martin, Charge radii and structural evolution in Sr, Zr, and Mo isotopes, Phys. Lett. B **691**, 202 (2010).
[33] J. E. García-Ramos and K. Heyde, Quest of shape coexistence in Zr isotopes, Phys. Rev. C **100**, 044315 (2019).
[34] J. E. García-Ramos and K. Heyde, Subtle connection between shape coexistence and quantum phase transition: The Zr case, Phys. Rev. C **102**, 054333 (2020).
[35] C. M. Baglin, Nuclear data sheets for A = 92, Nucl. Data Sheets **113**, 2187 (2012).
[36] D. Abriola and A. A. Sonzogni, Nuclear data sheets for A = 94, Nucl. Data Sheets **107**, 2423 (2006).
[37] A. Negret and A. A. Sonzogni, Nuclear Data Sheets for ^{94}Sr, http://www.nndc.bnl.gov/ensdf (2011).
[38] D. Abriola and A. A. Sonzogni, Nuclear data sheets for A = 96, Nucl. Data Sheets **109**, 2501 (2008).
[39] B. Singh and Z. Hu, Nuclear data sheets for A = 98, Nucl. Data Sheets **98**, 335 (2003).
[40] J. Chen and B. Singh, Nuclear data sheets for A=98, Nucl. Data Sheets **164**, 1 (2020).
[41] B. Singh, Nuclear data sheets for A = 100, Nucl. Data Sheets **109**, 297 (2008).
[42] D. DeFrenne, Nuclear data sheets for A = 102, Nucl. Data Sheets **110**, 1745 (2009).
[43] T. Rzaca-Urban, K. Sieja, W. Urban, F. Nowacki, J. L. Durell, A. G. Smith, and I. Ahmad, $(h_{11/2}, g_{7/2})_{9^-}$ neutron excitation in ^{92,94,96}Sr, Phys. Rev. C **79**, 024319 (2009).
[44] J. Park, A. B. Garnsworthy, R. Krücken, C. Andreoiu, G. C. Ball, P. C. Bender, A. Chester, A. Close, P. Finlay, P. E. Garrett, J. Glister, G. Hackman, B. Hadinia, K. G. Leach, E. T. Rand, S. Sjue, K. Starosta, C. E. Svensson, and E. Tardiff, Shape coexistence and evolution in ^{98}Sr, Phys. Rev. C **93**, 014315 (2016).
[45] E. Clément, M. Zielińska, A. Görgen, W. Korten, S. Péru, J. Libert, H. Goutte, S. Hilaire, B. Bastin, C. Bauer, A. Blazhev, N. Bree, B. Bruyneel, P. A. Butler, J. Butterworth, P. Delahaye, A. Dijon, D. T. Doherty, A. Ekström, C. Fitzpatrick *et al.*, Spectroscopic Quadrupole Moments in ^{96,98}Sr: Evidence for Shape Coexistence in Neutron-Rich Strontium Isotopes at $N = 60$, Phys. Rev. Lett. **116**, 022701 (2016).
[46] E. Clément and M. Zielińska, Shape coexistence in neutron-rich strontium isotopes at $N = 60$, Phys. Scr. **92**, 084002 (2017).
[47] J.-M. Régis, J. Jolie, N. Saed-Samii, N. Warr, M. Pfeiffer, A. Blanc, M. Jentschel, U. Köster, P. Mutti, T. Soldner, G. S. Simpson, F. Drouet, A. Vancraeyenest, G. de France, E. Clément, O. Stezowski, C. A. Ur, W. Urban, P. H. Regan, Zs. Podolyák *et al.*, Abrupt shape transition at neutron number $N = 60$: $B(E2)$ values in ^{94,96,98}Sr from fast γ-γ timing, Phys. Rev. C **95**, 054319 (2017); Erratum: Abrupt shape transition at neutron number $N = 60$: $B(E2)$ values in ^{94,96,98}Sr from fast γ-γ timing [Phys. Rev. C 95, 054319 (2017)], **95**, 069902(E) (2017).
[48] S. Cruz, P. C. Bender, R. Kruecken, K. Wimmer, F. Ames, C. Andreoiu, R. A. E. Austin, C. S. Bancroft, R. Braid, T. Bruhn, W. N. Catford, A. Cheeseman, A. Chester, D. S. Cross, C. Aa. Diget, T. Drake, A. B. Garnsworthy, G. Hackman, R. Kanungo, A. Knapton *et al.*, Shape coexistence and mixing of low-lying 0+ states in ^{96}Sr, Phys. Lett. B **786**, 94 (2018).
[49] A. Esmaylzadeh, J.-M. Régis, Y. H. Kim, U. Köster, J. Jolie, V. Karayonchev, L. Knafla, K. Nomura, L. M. Robledo, and R. Rodríguez-Guzmán, Lifetime measurements and shape coexistence in ^{97}Sr, Phys. Rev. C **100**, 064309 (2019).
[50] W. Urban, T. Rzaca-Urban, J. Wiśniewski, I. Ahmad, A. G. Smith, and G. S. Simpson, Structure of 0^+ excitations in the mass $A \approx 100$ region: 0_2^+ bands in ^{98}Sr and ^{100}Zr, Phys. Rev. C **99**, 064325 (2019).
[51] W. Urban, K. Sieja, T. Rzaca-Urban, J. Wiśniewski, A. Blanc, M. Jentschel, P. Mutti, U. Köster, T. Soldner, G. de France, G. S. Simpson, C. A. Ur, A. G. Smith, and J. P. Greene, Structure of even-even Sr isotopes with $50 \leqslant N \leqslant 58$ neutrons, Phys. Rev. C **104**, 064309 (2021).
[52] S. Cruz, K. Wimmer, S. S. Bhattacharjee, P. C. Bender, G. Hackman, R. Krücken, F. Ames, C. Andreoiu, R. A. E. Austin, C. S. Bancroft, R. Braid, T. Bruhn, W. N. Catford, A. Cheeseman, A. Chester, D. S. Cross, C. Aa. Diget, T. Drake, A. B. Garnsworthy, R. Kanungo *et al.*, Single-particle structure in neutron-rich Sr isotopes approaching the $N = 60$ shape transition, Phys. Rev. C **102**, 024335 (2020).
[53] F. Iachello and A. Arima, *The Interacting Boson Model* (Cambridge University Press, Cambridge, 1987).
[54] P. D. Duval and B. R. Barrett, Configuration mixing in the interacting boson model, Phys. Lett. B **100**, 223 (1981).
[55] P. D. Duval and B. R. Barrett, Quantitative description of configuration mixing in the interacting boson model, Nucl. Phys. A **376**, 213 (1982).
[56] D. D. Warner and R. F. Casten, Predictions of the interacting boson approximation in a consistent Q framework, Phys. Rev. C **28**, 1798 (1983).
[57] P. O. Lipas, P. Toivonen, and D. D. Warner, IBA consistent-Q formalism extended to the vibrational region, Phys. Lett. B **155**, 295 (1985).

[58] K. Heyde, P. Van Isacker, R. F. Casten, and J. L. Wood, A shell-model interpretation of intruder states and the onset of deformation in even-even nuclei, Phys. Lett. B **155**, 303 (1985).

[59] K. Heyde, J. Jolie, J. Moreau, J. Ryckebusch, M. Waroquier, P. Van Duppen, M. Huyse, and J. L. Wood, A shell-model description of 0+ intruder states in even-even nuclei, Nucl. Phys. A **466**, 189 (1987).

[60] J. E. García-Ramos and K. Heyde, The Pt isotopes: Comparing the interacting boson model with configuration mixing and the extended consistent-Q formalism, Nucl. Phys. A **825**, 39 (2009).

[61] J. E. García-Ramos, V. Hellemans, and K. Heyde, Platinum nuclei: Concealed configuration mixing and shape coexistence, Phys. Rev. C **84**, 014331 (2011).

[62] J. E. García-Ramos and K. Heyde, Nuclear shape coexistence: A study of the even-even Hg isotopes using the interacting boson model with configuration mixing, Phys. Rev. C **89**, 014306 (2014).

[63] J. E. García-Ramos and K. Heyde, Disentangling the nuclear shape coexistence in even-even Hg isotopes using the interacting boson model, in *Proceedings of the 15th International Symposium on Capture Gamma-Ray Spectroscopy and Related Topics (CGS15), Dresden, Germany, August 25–29, 2014* [EPJ Web Conf. **93**, 01004 (2015)].

[64] J. E. García-Ramos and K. Heyde, Nuclear shape coexistence in Po isotopes: An interacting boson model study, Phys. Rev. C **92**, 034309 (2015).

[65] J. E. García-Ramos and K. Heyde, The influence of intruder states in even-even Po isotopes, in *Nuclear Structure and Dynamics '15, 14–19 June 2015, Portorož, Slovenia*, edited by M. Lipoglavšek, M. Milin, T. Nikšić, S. Szilner, and D. Vretenar, AIP Conf. Proc. No. 1681 (AIP, New York, 2015), p. 040008.

[66] V. Hellemans, R. Fossion, S. De Baerdemacker, and K. Heyde, Configuration mixing in ^{188}Pb: Band structure and electromagnetic properties, Phys. Rev. C **71**, 034308 (2005).

[67] V. Hellemans, S. De Baerdemacker, and K. Heyde, Configuration mixing in the neutron-deficient $^{186-196}$Pb isotopes, Phys. Rev. C **77**, 064324 (2008).

[68] I. Angeli and K. P. Marinova, Table of experimental nuclear ground state charge radii: An update, At. Data Nucl. Data Tables **99**, 69 (2013).

[69] S. Zerguine, P. Van Isacker, and A. Bouldjedri, Consistent description of nuclear charge radii and electric monopole transitions, Phys. Rev. C **85**, 034331 (2012).

[70] R. Fossion, C. DeÂ Coster, J. E. García-Ramos, T. Werner, and K. Heyde, Nuclear binding energies: Global collective structure and local shell-model correlations, Nucl. Phys. A **697**, 703 (2002).

[71] S. Sachdev, *Quantum Phase Transitions* (Cambridge University Press, Cambridge, 2011).

[72] J. N. Ginocchio and M. W. Kirson, An intrinsic state for the interacting boson model and its relationship to the Bohr-Mottelson model, Nucl. Phys. A **350**, 31 (1980).

[73] A. E. L. Dieperink and O. Scholten, On shapes and shape phase transitions in the interacting boson model, Nucl. Phys. A **346**, 125 (1980).

[74] A. E. L. Dieperink, O. Scholten, and F. Iachello, Classical Limit of the Interacting-Boson Model, Phys. Rev. Lett. **44**, 1747 (1980).

[75] R. Gilmore, *Lie Groups, Lie Algebras and Some Applications* (Wiley, New York, 1974).

[76] A. Frank, O. Castaños, P. Van Isacker, and E. Padilla, The geometry of the IBM with configuration mixing, in *Mapping the Triangle: International Conference on Nuclear Structure, 22–25 May 2002, Grand Teton National Park, Wyoming*, AIP Conf. Proc. No. 638 (AIP, New York, 2002), p. 23.

[77] A. Frank, P. Van Isacker, and C. E. Vargas, Evolving shape coexistence in the lead isotopes: The geometry of configuration mixing in nuclei, Phys. Rev. C **69**, 034323 (2004).

[78] A. Frank, P. Van Isacker, and F. Iachello, Phase transitions in configuration mixed models, Phys. Rev. C **73**, 061302(R) (2006).

[79] I. O. Morales, A. Frank, C. E. Vargas, and P. Van Isacker, Shape coexistence and phase transitions in the platinum isotopes, Phys. Rev. C **78**, 024303 (2008).

[80] J. E. García-Ramos, K. Heyde, L. M. Robledo, and R. Rodríguez-Guzmán, Shape evolution and shape coexistence in Pt isotopes: Comparing interacting boson model configuration mixing and Gogny mean-field energy surfaces, Phys. Rev. C **89**, 034313 (2014).

[81] K. Kumar, Intrinsic Quadrupole Moments and Shapes of Nuclear Ground States and Excited States, Phys. Rev. Lett. **28**, 249 (1972).

[82] D. Cline, Nuclear shapes studied by Coulomb excitation, Annu. Rev. Nucl. Part. Sci. **36**, 683 (1986).

[83] Y. Alhassid, C. N. Gilbreth, and G. F. Bertsch, Nuclear Deformation at Finite Temperature, Phys. Rev. Lett. **113**, 262503 (2014).

[84] C. N. Gilbreth, Y. Alhassid, and G. F. Bertsch, Nuclear deformation in the laboratory frame, Phys. Rev. C **97**, 014315 (2018).

[85] M. T. Mustonen, C. N. Gilbreth, Y. Alhassid, and G. F. Bertsch, Statistical theory of deformation distributions in nuclear spectra, Phys. Rev. C **98**, 034317 (2018).

[86] A. Poves, F. Nowacki, and Y. Alhassid, Limits on assigning a shape to a nucleus, Phys. Rev. C **101**, 054307 (2020).

[87] J. Srebrny, T. Czosnyka, Ch. Droste, S. G. Rohoziski, L. Próchniak, K. Zajac, K. Pomorski, D. Cline, C. Y. Wu, A. BÃ¤cklin, L. Hasselgren, R. M. Diamond, D. Habs, H. J. Körner, F. S. Stephens, C. Baktash, and R. P. Kostecki, Experimental and theoretical investigations of quadrupole collective degrees of freedom in ^{104}Ru, Nucl. Phys. A **766**, 25 (2006).

[88] E. Clément, A. Görgen, W. Korten, E. Bouchez, A. Chatillon, J.-P. Delaroche, M. Girod, H. Goutte, A. Hürstel, Y. Le Coz, A. Obertelli, S. Péru, Ch. Theisen, J. N. Wilson, M. Zielińska, C. Andreoiu, F. Becker, P. A. Butler, J. M. Casandjian, W. N. Catford *et al.*, Shape coexistence in neutron-deficient krypton isotopes, Phys. Rev. C **75**, 054313 (2007).

[89] K. Wrzosek-Lipska, L. Próchniak, M. Zielińska, J. Srebrny, K. Hadynska-Klek, J. Iwanicki, K. M., M. Kowalczyk, P. J. Napiorkowski, D. Pietak, and T. Czosnyka, Electromagnetic properties of ^{100}Mo: Experimental results and theoretical description of quadrupole degrees of freedom, Phys. Rev. C **86**, 064305 (2012).